Supplemental Information

Patterns and Processes in Aerosol Deposition: Insights from a 9-year Study of ^{7}Be, ^{210}Pb, Sulfate and Major/Trace Elements

Joshua D. Landis[1*], Xiahong Feng[1], James M. Kaste[2], and Carl E. Renshaw[1]
[1]Department of Earth Sciences, Dartmouth College, 6105 Fairchild Hall, Hanover, NH 03755, USA;
[2]Geology Department, The College of William and Mary, McGlothlin-Street Hall 217, Williamsburg, VA 23187, USA.

*Corresponding author: Joshua Landis (joshua.d.landis@dartmouth.edu)

Supplemental Information consists of the following components:

Supplemental Discussion

1.1. Principle Component Analysis to characterize FRN/MTE aerosol chemistries

We first used Principal Component Analysis (PCA) to optimize the separation of mean FRN and MTE depositional fluxes in an empirical coordinate space. In addition to 17 FRNs/MTEs, in this analysis we included m and p_D as representative end-members for dust and condensation nuclei, respectively. PCA was performed with the correlation matrix, and we removed 34 outliers that were flagged through the JMP14.0 algorithm.

The first principal component (PC1) explained 45% of variance in the data set but weighted all FRNs/MTEs similarly and did not provide useful separation of variables. We interpreted PC1 as the commonality among FRN and MTE fluxes due to deposition via m_C and p_D, mutual enrichment in E-type storms [$p<0.05$], and depletion in winter [$p<0.05$] [multiple regression $R^2=0.67$, $p<0.0001$; m_C= 42%, p_D=12%, storm = 7%, season=6%]. Two other PCs together provided strong separation of variables, PC2 (17% variance) and PC3 (8% variance). PC2 was correlated with log(m_C) [$R^2=0.67$, $p<0.0001$] and thus discriminates aerosols based on wet/dry deposition. PC3 was most strongly controlled by summer/winter seasonality [$R^2=0.26$, $p<0.0001$; $0^A > 3^B > 1^B > 2^C$, $p<0.05$].

We used the impute missing data function in JMP14.0 PCA platform to hindcast missing data for N^P, C^P since these did not span the full 9-year FRN data set (3 years data, n=151 for C, N) and Hg (6 years data, n=273 for Hg). This allowed us to reinsert imputed N^P, C^P and Hg into PCA with the full FRN/MTE data set, without changing relationships among the variables. We also used imputed data for subsequent multiple regressions, but in these instances (e.g., multiple regression for ^{7}Be with ^{210}Pb, N^P, p_D, season, storm type and season as explanators) the response variable and others in its aerosol type (^{7}Be, ^{210}Pb, S and p_D) were omitted from the PCA imputation to prevent any circularity in the imputed data. For these instances we cite the p-value for the multiple regressions using only measured data, but then use imputed data in the final regression when citing p-values and coefficients for other explanators.

Whereas PCA found the best discrimination among all variable means, we also wanted to understand relationships among individual MTEs since this would better reveal contributions distinct types of aerosols in bulk deposition. To do this we used step-wise multiple regression models for each individual FRN/MTE, with 18 remaining variables plus season as explanators. From the many interactions among FRNs/MTEs we constructed a correlation web to illustrate correlations that are buried in higher dimensions of the PCA.

We classified FRNs/MTEs in bulk deposition according to aerosol type as follows:

1. secondary aerosol: ^{7}Be, ^{210}Pb and S all are produced in the atmosphere by gas-particle conversion via cosmogenic spallation, radiogenic decay, or SO_2 oxidation, respectively. p_D grouped with the FRNs and S, consistent with the control of condensation and scavenging on deposition of secondary aerosols. Some discrimination among the secondary aerosols emerged from CNA, too. ^{210}Pb shared an independent correlation with S, which is consistent with formation of $PbSO_4$ (*Biggins and Harrison 1979*). ^{7}Be did not show this relationship with S (Figure 3b). Conversely, ^{7}Be shared an independent correlation with p_D whereas ^{210}Pb did not (Figure 3b). In multiple linear regression, Zn, N^P and K also included significant correlations with p_D.

2. biogenic aerosol: The combination of N, P and K is typical of biogenic aerosols that include vegetative debris and pollen (*Creamean et al. 2014*), as well as fertilizer application to agricultural fields (*Tositti et al. 2018*). Soil and biomass combustion can also include K (*Shen et al. 2019*). Mn appears transitional between biogenic and mineral aerosols, with significant correlations with Mg as well as P, K and particulate nitrogen (N^P). Regarding biogenic origins, Mn is strongly cycled through vegetation and forest canopies (*Rea et al. 2001*), and it is estimated that 95% of Mn-oxides are biologically produced

(*Villalobos et al. 2005*). Our mean C:N ratio of ~16 (Landis et al. in review) is similar to PM10 reported in natural environments and not enriched as from resuspension of tilled soil.

3. anthropogenic aerosol: Zn, V and Hg are recognized atmospheric pollutants, Hg predominately from fossil fuel combustion and gaseous re-evasion from natural reservoirs (*Driscoll et al. 2013, Eckley et al.2016*), Zn from both combustion and automobile tire wear (*Gonzalez et al. 2016*), and V from fuel combustion (*Chen and Duce Atm. Env. 1983, Shafer et al. EST 2012*). Higher deposition of Zn, V and Hg in cool seasons reflects increased production through winter heating (e.g., *Chen and Duce 1983*), while Hg may also be depressed in summer due to biological uptake (*Jiskra et al. 2018*). While Na is not an atmospheric pollutant, its affinity for this group is attributable to a winter bias due to de-icing roads and sidewalks with salts as is common across the New England region (*Dugan et al. 2017*). Sulfur has significant correlations to each of V, Zn and Hg, consistent with a combustion source of S (*Batonneau et al. 2004*).

4. insoluble mineral aerosol: Fe and Al represent primary aerosols and particles eroded and resuspended from lithogenic materials. Fe was correlated weakly to m_D and anti-correlated with p_D. Consistent with lithogenic dust, both Fe and Al were sparingly soluble without acidification of the bulk collector.

5. soluble mineral aerosol: Ca, Sr and Mg were dominated by dry deposition but were also relatively soluble. Ca and Sr had strong correlations to S, suggesting the presence of soluble $CaSO_4$ and $SrSO_4$. Mg was most strongly correlated with Mn, P and Fe, suggesting a mixture of biogenic and lithogenic contributions.

1.2. Discriminant Analysis to generate multi-event storm classes

We used the discriminant analysis platform in JMP14.0 to delineate empirical classifications of sample collections using a mixing-plot approach with log(^{7}Be), log(^{210}Pb) and log(^{7}Be:^{210}Pb) as covariates. We then used this approach to extend the *E-N-D* classification based on single-event collections to the full dataset that includes multi-event collections. This created new classes N^m, E^m or D^m. We used the default quadratic method (unequal variances among groups), with percent misclassified =2.6% and entropy R^2 0.922. We reclassified 20 D^m samples that were misclassified according to their nearest-neighbor *D* samples.

1.3. MANOVA to compare storm-type MTE compositions

We evaluated MTE compositions of the *E-N-D* event types using Multiple Analysis of Variance (MANOVA), which compares all FRNs/MTEs simultaneously as vectors. FRNs were omitted since these were used to define the *E-N-D* grouping. We prepared MTE data by regressing log(s_i) vs. log(p_D), where s_i indicates concentration of the MTE soluble fraction (mg L^{-1}). From regressions we fit orthogonals and analyzed residuals to remove the influence of precipitation depth. We found that *E-N-D* event types have distinct chemical compositions, with each event type significantly different than the other two [$p<0.0001$]. We followed with ANOVA to assess storm-type differences for individual FRNs and MTEs as reported in the manuscript.

1.4. Mass balance constraints on ^{210}Pb deposition

The ^{210}Pb ecosystem mass balance is complicated by uncertainties in how atmospheric or excess ^{210}Pb ($^{210}Pb_{ex}$) is resolved from the geogenic or supported fraction of ^{210}Pb in soils – the same Rn emanation process that produces atmospheric ^{210}Pb globally results in some local *in situ* deficit in supported ^{210}Pb in the field and in the analytical hand sample. These deficits may be significant, commonly in the range of 10-30% (*e.g., Landis et al. 2016*). While our own mass balance incorporates an explicit correction for ^{210}Pb deficit, its underestimation would produce a concomitant overestimation of recycled deposition to the bulk collector.

At the same time, error in the estimation of $^{210}Pb_{ex}$ might be offset by contributions of ^{210}Pb to forest soils via dry deposition to the overlying tree canopy. On an areal basis, dry deposition of ^{210}Pb and accumulation-mode aerosols is likely to be greater to a canopy of vegetation than to the bulk collector due to surface roughness of leaves, micrometeorological phenomena of air flow through the canopy, and a high Leaf Area Index (LAI) (e.g., *Yamamoto et al. 1998*). LAI is the cumulative projected leaf surface area per unit ground surface area. If dry deposition to the canopy is higher than to the bulk collector, then the recycled contribution to the bulk collector would be underestimated by a corresponding amount. A final caveat, however -- it has not been established what fraction of FRN dry deposition to the canopy may be recycled, and as for MTEs it is likely to be significant.]

1.5. Global deposition data.

In global data for the North America/Europe (NAE) and Southeast/East Asian (SEA) regions, we found only weak or absent correlations of ^{7}Be:^{210}Pb with latitude [R^2=0.17, p=0.014] or p_D [R^2=0.00, p=0.97]. Similarly, there was no significant influence of latitude on ^{7}Be flux alone in global data [R^2=0.07, p=0.13]. However, we found a strong regional effect []

Analyzing by region, we found a strong correlation of ^{7}Be:^{210}Pb with p_D in the NAE region, driven by ^{7}Be fluxes which increased strongly with p_D [14.5 ±3.1 Bq m^{-2} y^{-1} cm^{-1}; R_a^2=0.41, p<0.0001, *n*=31]. No effect was present for ^{210}Pb [R_a^2=-0.03, *p*=0.88; mean flux =137 ±10 Bq m^{-2} y^{-1}; mean +SE, *n*=31]. When we modeled FRN fluxes with p_D, latitude and longitude as explanators, only p_D is predictive for ^{7}Be [p<0.0001]. There is no effect from latitude despite its control on ^{7}Be production [p=0.47]. For ^{210}Pb there is a significant decline with longitude attributable to low production in the Atlantic Ocean [R^2=0.28, p=0.017]

Conversely, low-latitude SEA sites show no control of p_D on ^{7}Be:^{210}Pb ratios.
^{7}Be increased only gradually with annual precipitation [3.4 ±1.2 Bq m^{-2} y^{-1} cm^{-}1; R_a^2=0.18, p=0.008, *n*=32)]. ^{210}Pb did not increase with precipitation [R_a^2=0.08, *p*=0.57; mean =234 ±25 Bq m^{-2} y^{-1}].

SEA sites on the Sea of Japan (SEA-j) are a notable exception from other SEA sites. For these sites ^{7}Be increased strongly with p_D [28.7 ±5.9 Bq m^{-2} y^{-1} cm^{-1}; R_a^2=0.79, p=0.005, *n*=7], as did ^{210}Pb [3.4 ±1.6 Bq m^{-2} y^{-1} cm^{-1}; R_a^2=0.36, p=0.09, *n*=7]. The SEA-j sites have exceedingly high ^{7}Be and ^{210}Pb fluxes due to a combination of factors, including strong winter monsoons that deliver Asian continental air and an orographic effect on the western coast of Japan (*Tokeida et al. 1996*, *Yamamoto et la. 2006*).

Interannual variability of ^{7}Be:^{210}Pb vs. p_D for global sites: Hanover, NH USA (R_a^2=-0.13, *p*=0.82, *n*=9; *this study*); Malaga, Spain (R_a^2=-0.10, *p*=0.75, *n*=11; *Duenas et al.*), Monaco (R_a^2=-0.09, p=0.77, *n*=13; *Pham et al.*), Rokkasho, Japan (R_a^2=-0.27, p=0.73, *n*=5; *Akata et al.*), Shanghai, China (R_a^2=-0.11, p=0.57, *n*=7; *Du et al.*), Tatsunokuchi, Japan (R_a^2=-0.07, p=0.66, *n*=12; *Yamamoto et al. 2006*).

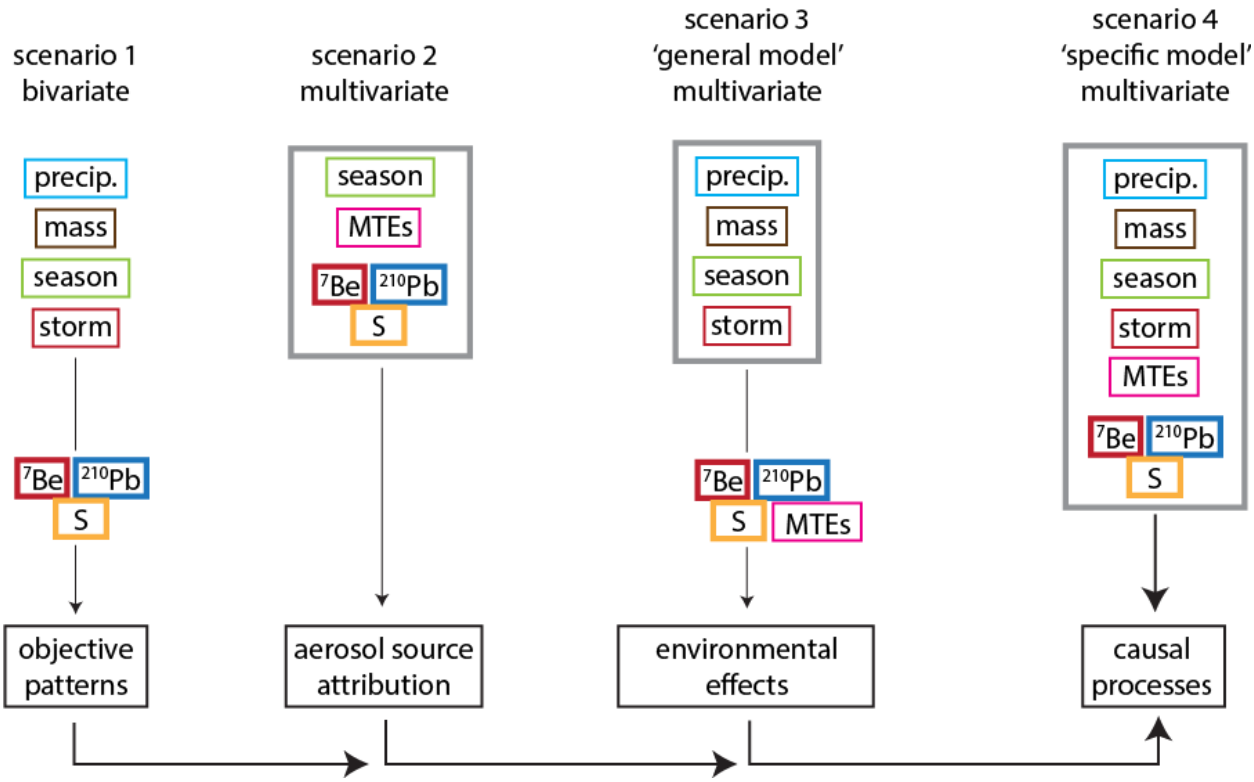

Figure SI 1a: flowchart for statistical analyses, where bivariate relationships are first used to describe objective patterns in 7Be and 210Pb deposition, attributable to general environmental factors (scenario 1). A second series of multiple regressions use major/trace elements (MTEs) and fallout radionuclides (FRNs) to identify aerosol types that contributed to their bulk deposition (scenario 2). Multivariate models are then introduced to isolate FRN controls related to general factors from those intrinsic to each FRN (scenarios 3 and 4).

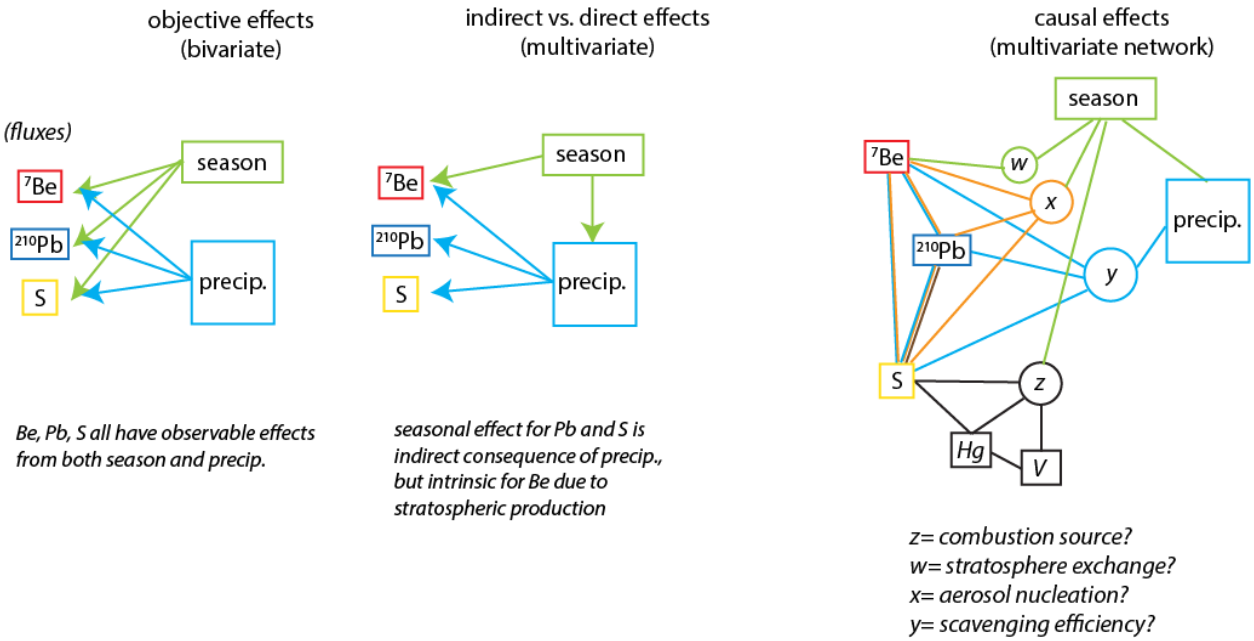

Figure SI 1b: inferring causal processes from statistical models.

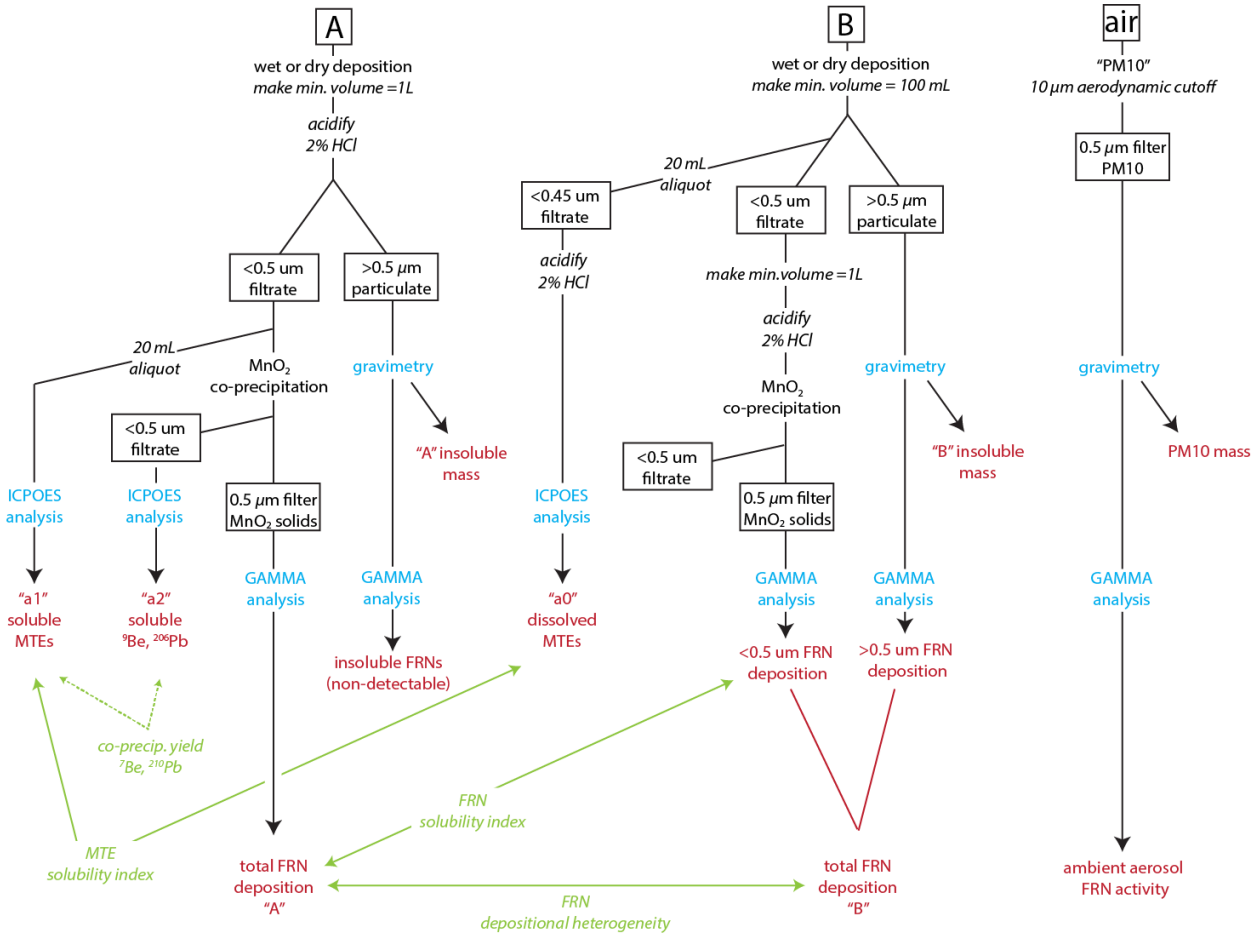

Figure SI 2: methods flowchart for analysis of fallout radionuclides (FRNs) and major/trace elements (MTEs) in bulk deposition.

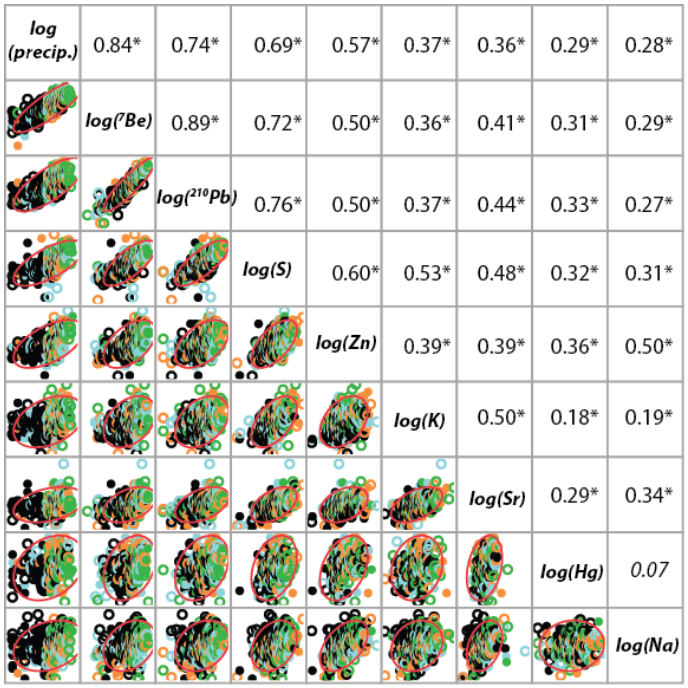

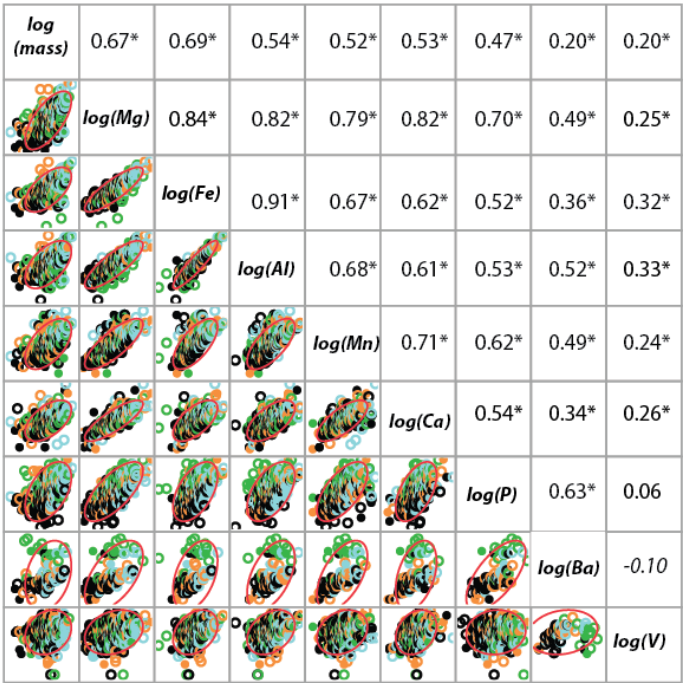

Figure SI 3: multivariate correlation plots for elements with strongest prediction by precipitation depth (a) or dust mass (b). Correlation R2 is indicated, and * indicates significant at $p<0.0001$. Data are coded by season with black =winter, blue =spring, green =summer, orange =fall. Open symbols indicate single-storm collections, closed symbols indicate multi-storm collections.

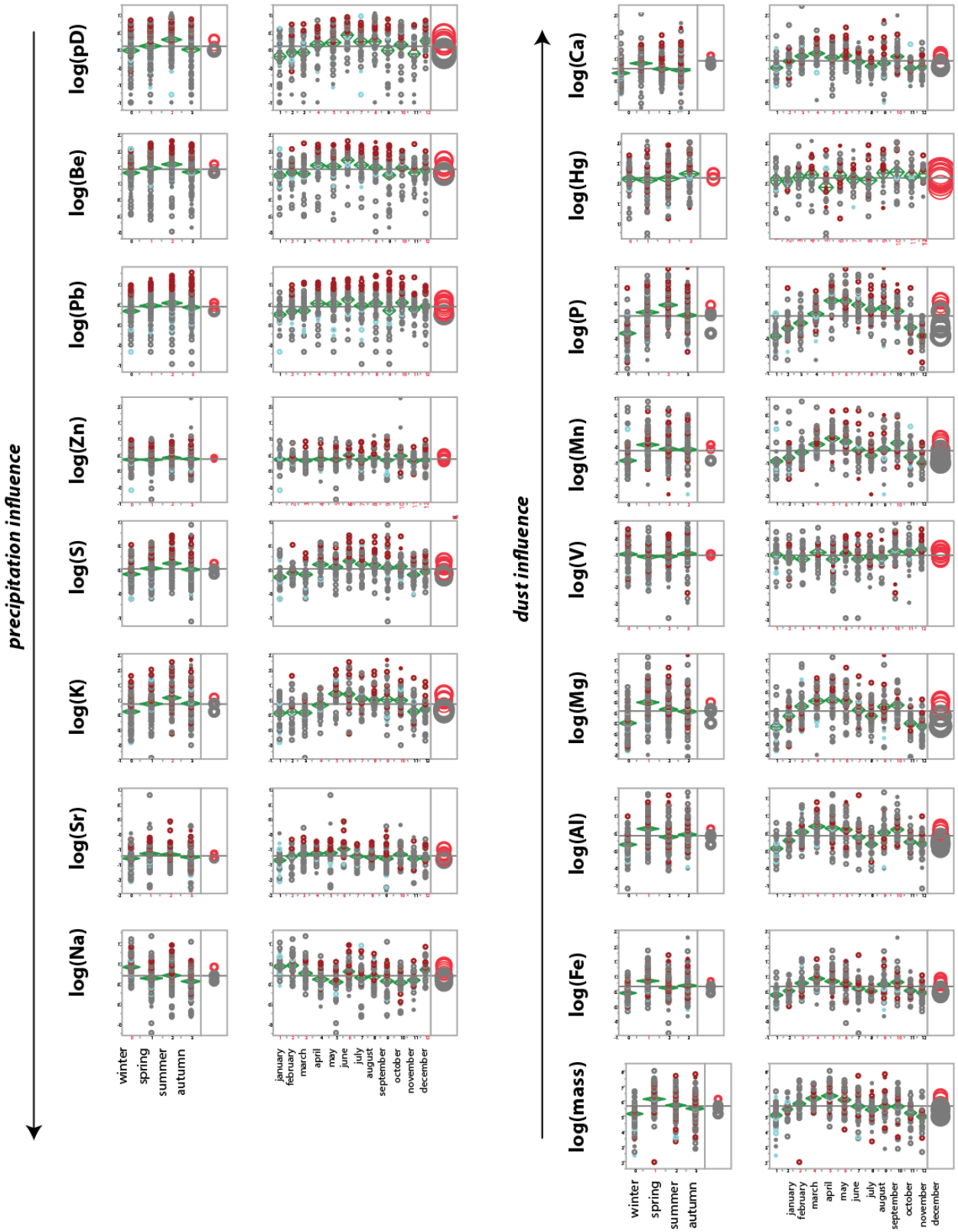

Figure SI 4: monthly and seasonal ANOVA for bulk deposition parameters.

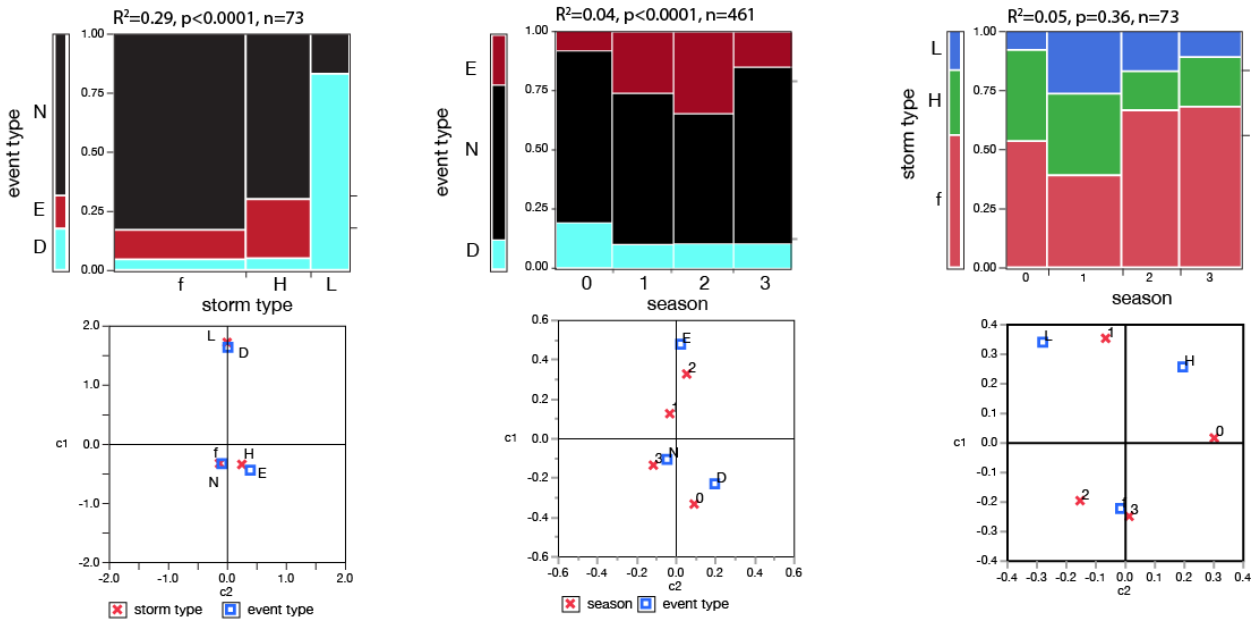

Figure SI 5 (a) correspondence analysis for empirical storm type (E, N, D) versus meteorological type (H, f, L); (b) correspondence analysis for storm type versus season; (c) correspondence analysis for meteorological type versus season.

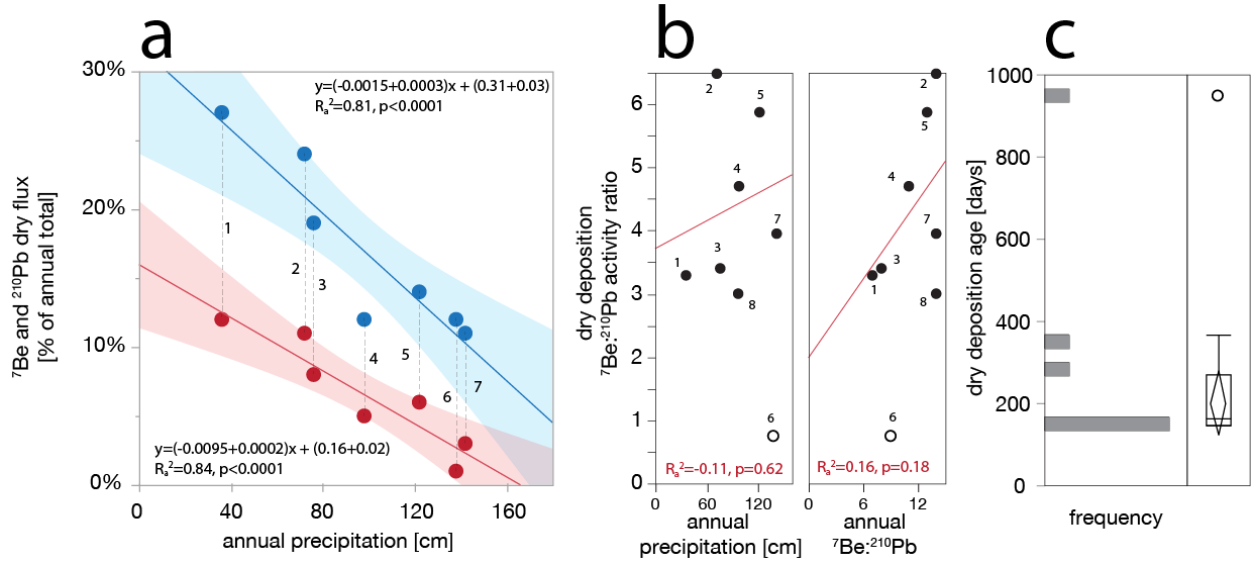

Figure SI 6: (a) contribution of dry deposition to annual fluxes of ^{7}Be (red) and ^{210}Pb (blue). Solid lines indicate linear best fits, shaded bands indicate confidence bands (95%). (b) ^{7}Be:^{210}Pb ratios of dry deposition versus annual precipitation and annual flux ratio. Lines show linear best fits. (c) frequency distribution of dry deposition ages calculated with an open-system accumulation model and assuming an initial ^{7}Be:^{210}Pb ratio equal to total annual deposition (Landis et al. 2014. Mean age = 201 ±32 days (±SD, *n*=7). Data sources are: 1, Duenas et al. (2011); 2, Lozano et al. (2011); 3, McNeary and Baskaran (2003); 4, Landis et al. herein; 5, Baskaran (1993); 6, Benitez-Nelson and Buesseler (1999); 7, Baskaran and Swarzenski (2007). Site 6 (open circle) was omitted as outlying from analyses in (b) and (c).

Table SI 1 - multiple regression of general environmental factors on FRN and MTE deposition

model response				p_D [1]			m_D [2]			season			storm type		
	R^2	RMSE	*p*	e*[3]	m*[4]	*p*	e*	m*	*p*	e*	m*	*p*	e*	m*	*p*
log ^{7}Be:^{210}Pb	0.50	0.14	<0.0001	22%	14%	<0.0001	0.0%	0.1%	0.817	2%	20%	<0.0001	26%	193%	<0.0001
log ^{7}Be	0.73	0.25	<0.0001	70%	60%	<0.0001	1%	3%	0.009	1%	32%	0.0023	2%	49%	<0.0001
log ^{210}Pb	0.73	0.21	<0.0001	51%	36%	<0.0001	1%	2%	0.014	1%	18%	*0.072*	20%	270%	<0.0001
log(S)	0.56	0.19	<0.0001	36%	20%	<0.0001	5%	4%	<0.0001	1%	18%	*0.070*	13%	112%	<0.0001
log N^P	0.59	0.32	<0.0001	12%	20%	<0.0001	32%	45%	<0.0001	15%	167%	<0.0001	0.0%	2%	0.99
log C^P	0.59	0.27	<0.0001	8%	20%	0.0002	48%	45%	<0.0001	3%	45%	0.17	0.0%	0.9%	0.97
log Zn	0.35	0.20	<0.0001	27%	16%	<0.0001	4%	3%	<0.0001	0%	2%	0.99	4%	49%	0.0001
log K	0.33	0.37	<0.0001	7%	15%	<0.0001	11%	11%	<0.0001	10%	114%	<0.0001	4%	74%	0.0002
log Na	0.31	0.28	<0.0001	6%	12%	<0.0001	3%	5%	<0.0001	20%	157%	<0.0001	2%	37%	0.0043
log Hg	0.1	0.36	<0.0001	4%	10%	0.004	2%	5%	0.038	3%	52%	0.046	4%	100%	0.016
log Sr	0.40	0.26	<0.0001	4%	8%	<0.0001	26%	13%	<0.0001	0.3%	11%	0.68	11%	130%	<0.0001
log P	0.50	0.33	<0.0001	2%	7%	0.004	21%	16%	<0.0001	25%	282%	<0.0001	3%	58%	0.0007
log Ca	0.49	0.19	<0.0001	4%	6%	<0.0001	35%	11%	<0.0001	4%	33%	<0.0001	7%	61%	<0.0001
log V	0.13	0.34	<0.0001	0.7%	5%	0.055	6%	9%	<0.0001	5%	76%	<0.0001	2%	104%	0.0042
log Mn	0.58	0.27	<0.0001	0.8%	4%	0.022	42%	20%	<0.0001	11%	113%	<0.0001	4%	77%	<0.0001
log Mg	0.58	0.22	<0.0001	0%	-1%	0.33	49%	17%	<0.0001	5%	58%	<0.0001	4%	68%	<0.0001
log Al	0.37	0.32	<0.0001	0.5%	-3%	*0.11*	27%	16%	<0.0001	6%	60%	<0.0001	3%	54%	0.0006
log Fe	0.48	0.26	<0.0001	1.3%	-5%	0.007	41%	17%	<0.0001	4%	50%	<0.0001	2%	43%	0.0047

[1] p_D is precipitation depth

[2] m_D is mass deposition

[3] e^* is the net effect on response variable variance, with sum(e^*) = R^2

[4] m^* is the net change upon doubling of explanator, or difference in means between categories

Table SI 2: Multiple Regressions of Specific Factors on ^{7}Be, ^{210}Pb and S Bulk Deposition

log Be	R^2	RMSE	*p*		**log Pb**	R^2	RMSE	*p*		**log S**	R^2	RMSE	*p*	
model	0.91	0.13	<0.0001		*model*	0.90	0.13	<.0001*		*model*	0.69	0.15	<.0001*	
explanator	e*[a]	m*[b]	*p*	VIF	*explanator*	e*	m*	*p*	VIF	*explanator*	e*	m*	*p*	VIF
log Pb	64%	84%	<0.0001	3.4	log Be	73%	53%	<0.0001	1.6	log Pb	32%	25%	<0.0001	2.4
log p_D[c]	13%	18%	<0.0001	2.5	storm type	15%	312%	<0.0001	1.5	log P	15%	10%	<0.0001	1.5
storm type	11%	155%	<0.0001	2.9	log S	1.3%	9%	<0.0001	1.8	log Ca	8%	13%	<0.0001	1.7
season	1.7%	20%	0.0002	1.1						log V	7%	7%	<0.0001	1.1
log sunspot	0.8%	-2%	0.0029	1.4						log p_D	4%	6%	0.0003	2.3
log N^P	0.7%	4%	0.0054	1.0						log Na	3%	6%	0.0029	1.2

[a] *e** is the net effect on response variable variance, with sum(*e**) = R^2

[b] *m** is the net change upon doubling of explanator, or difference in means between categories

[c] p_D is precipitation depth